

REALISTIC TRANSMISSION MODEL OF ROUGH SURFACES

Huiying Xu and Yinlong Sun

Department of Computer Sciences, Purdue University, West Lafayette, Indiana 47907, USA

Keywords: Transmission model, BTDF, rough surface, Monte Carlo simulation, light scattering.

Abstract: Transparent and translucent objects involve both light reflection and transmission at surfaces. This paper develops a realistic transmission model of rough surfaces using the statistical ray method, which is a physically based approach that has been developed recently. The surface is assumed locally smooth and statistical techniques can be applied to calculate light transmission through a local illumination area. We have obtained an analytical expression for single scattering. The analytical model has been compared to our Monte Carlo simulations as well as to the simulations by others, and good agreements have been achieved. The presented model has a potential for realistic rendering of transparent and translucent objects.

1 INTRODUCTION

Light scattering by objects is generally characterized by a *bidirectional scattering distribution function* (BSDF) (Glassner, 1995)

$$\rho(\theta_i, \varphi_i, \theta_o, \varphi_o, \lambda) = \frac{dL_o(\theta_o, \varphi_o, \lambda)}{L_i(\theta_i, \varphi_i, \lambda) \cos \theta_i d\Omega_i}, \quad (1)$$

which is the ratio of the scattered radiance dL_o in the outgoing direction (θ_o, φ_o) to the irradiance $L_i \cos \theta_i d\Omega_i$ in the direction (θ_i, φ_i) (Figure 1) at wavelength λ . When referring to reflection or transmission, a BSDF becomes a *bidirectional reflectance distribution function* (BRDF) or a *bidirectional transmittance distribution function* (BTDF). This paper studies the case of transmission.

In computer graphics application, materials may be classified into three major types: opaque, transparent and translucent. An opaque object only involves reflection, a transparent object involves both reflection and transmission, and a translucent object has volumetric scattering in addition to reflection and transmission at the object surface. Thus, a transmission model is needed for not only transparent but also translucent objects. Such objects include glass wares, plastics, ices, biological tissues, marbles, waxes, and so on.

There has been extensive research on modelling BRDFs in computer graphics, but studies on BTDFs are limited. Different from at an opaque surface, a scattering process at a surface of some transparent or translucent material is generally a combination of reflection and transmission events, and the number

of the events may be one (single scattering), two or more (multiple scattering). Solving the case of single scattering is a basis for solving the case of multiple scattering.

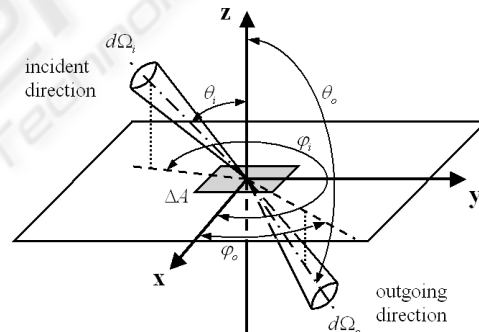


Figure 1: Light scattering at a surface (transmission case).

This paper presents a realistic transmission model of rough surfaces. The model is derived using a physically based approach called the statistical ray method that has been developed recently by Sun (2007). The key assumption of the surface is that the surface is sufficiently smooth locally and statistical techniques can be applied to calculate light transmission through a local illumination area. We have obtained an analytical expression for single scattering. The model has been compared to our Monte Carlo simulations as well as to the simulations by others, and good agreements have been achieved.

2 BACKGROUND

Existing BRDF models commonly consist of the diffuse and specular terms. The diffuse component is typically Lambertian, but the specular term differs in various models. A simple approach describes the specular component with an empirical function, such as the models of Phong (1975), Ward (1992), and Lafortune (1997).

Deriving accurate models needs physically based approaches. One approach uses the Kirchhoff theory with the tangent plane approximation of the surface (Beckmann, 1963; He, 1991). Another approach is based on the microfacet assumption of Torrance and Sparrow (1967). In this approach, the specular term is expressed as a product of the Fresnel coefficient, masking and shadowing factor, and surface orientation probability (Blinn, 1977; Cook and Torrance, 1982). Ashikhmin et al. (2000) developed an analytic model to remove the limitation of V-shaped grooves needed for the traditional microfacet model. Recently, Sun (2007) proposed a statistical ray method for deriving illumination models of rough surfaces. This method will be employed to model light transmission in this paper.

To our best knowledge, two transmission models exist in computer graphics. The first was proposed by He (1993) based on the Kirchhoff theory, and the second by Stam (2001) as an extension from Cook-Torrance's reflection model (1982). In practice, the rendering of light transmission is rather simple, typically based on a formula that extends Phong's reflection model to the case of transmission.

Beyond computer graphics, some research has been conducted to numerically simulate transmission. One example is the work of Nieto-Vesperinas et al. (1990) where light transmission at rough surfaces was computed using a Monte Carlo method.

Since transmission at a surface is a part of the problem of object translucency, we briefly review some research on translucency models. Hanrahan and Krueger (1993) developed a pioneering model of subsurface scattering using the linear transport theory. Jensen and Christensen (1998) studied light transport in participating media using Monte Carlo bi-directional ray tracing and volumetric photon mapping. Dorsey et al. (1999) simulated subsurface scattering of weathered stones using Monte Carlo ray tracing. Pharr and Hanrahan (2000) developed a Monte Carlo approach to solve generic scattering equations. Stam (2001) used the radiative transfer equation to model subsurface scattering of human skins. Koenderink and van Doorn (2001) studied subsurface scattering with a diffusion approximation of light transport theory. Jensen et al. (2001)

proposed an analytic model of BSSRDF, and later Jensen et al. (2002) developed a two-pass technique to efficiently render translucent objects. Recently, Wang et al. (2005) presented a technique based on pre-computed light transport to render translucent objects, and Mertens et al. (2005) proposed an efficient algorithm to render the local effect of subsurface scattering. These studies focused on the subsurface or volumetric scattering, and light transmission at the surface was not considered.

3 ANALYTICAL MODELING

Light transmission processes at a rough surface can be classified into single and multiple scattering. In single scattering (ray 1 in Figure 2), a light ray is scattered one time (this is in fact a refraction at the local area). In multiple scattering (ray 2 or 3 in Figure 2), there are multiple times of reflection and transmission. The total BTDF may be expressed as

$$\rho_{\text{total}} = \rho_{\text{single}} + \rho_{\text{multiple}}, \quad (2)$$

where ρ_{single} and ρ_{multiple} are the contributions from single and multiple scattering, respectively.

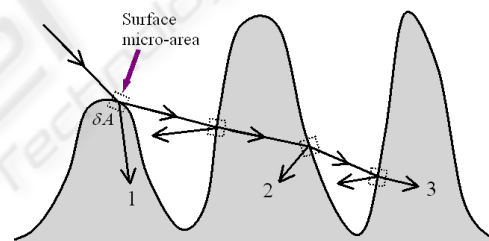


Figure 2: Light transmission processes of single scattering (ray 1) and multiple scattering (rays 2 and 3).

Now we use the statistical ray method proposed by Sun (2007) to calculate light transmission at a rough surface. The assumptions and conditions of our considered surface are similar to those used by Sun (2007) where the focus was on reflection, but now the focus is on transmission. For convenience, the assumptions are listed below:

1. Any surface micro-area δA has size much larger than wavelength and is sufficiently smooth such that it can be replaced with its local tangent plane.
2. Any local illumination area ΔA for the definition of BTDF (Figure 1) contains many surface micro-areas δA . As a result, it is valid to use the concept of probability of micro-areas δA within ΔA .
3. The surface properties remain the same in ΔA . These properties include the material aspect such as the optical constants, and the geometric aspect such as the statistics of the surface profile.

4. The surface profile is a height field. That is, for any line parallel with the z-axis, the line will intersect with the surface profile exactly one time.
5. A combined probability can be approximated as a product of the individual probabilities (see below).
6. The correlation between the incident and outgoing directions are ignored.

As additional conditions, we assume that the surface is isotropic and has a Gaussian height probability density and correlation function.

Since the surface is a Gaussian height field, the probability density function of surface height is

$$p(\zeta) = \frac{1}{\sqrt{2\pi}\sigma} \exp(-\zeta^2/2\sigma^2), \quad (3)$$

where ζ is the surface height, and σ is the standard deviation or RMS.

To describe surface roughness, we need to consider the surface height correlation. A two-point correlation function is generally defined as

$$C(\mathbf{r}) = \langle h(\mathbf{r}_0)h(\mathbf{r}_0 + \mathbf{r}) \rangle / \sigma^2, \quad (4)$$

which involves the average of the product of heights at points \mathbf{r}_0 and $\mathbf{r}_0 + \mathbf{r}$ on the $z=0$ plane. Since the surface is homogeneous (Assumption 3), the correlation is independent of \mathbf{r}_0 . Also, because the surface is isotropic, we can write $C(\mathbf{r}) = C(r)$. A common form of $C(r)$ is Gaussian, i.e.

$$C(r) = \exp(-r^2/\tau^2), \quad (5)$$

where τ is the correlation length. Now we define the surface smoothness as

$$s = \tau / \sigma. \quad (6)$$

The smaller is s , the rougher the surface; vice versa.

Given surface profile $\zeta = h(x, y)$, the orientation of a micro-area δA is described by the partial derivatives (ζ'_x, ζ'_y)

$$\zeta'_x = \frac{\partial h(x, y)}{\partial x}, \quad \zeta'_y = \frac{\partial h(x, y)}{\partial y}. \quad (7)$$

From Sun (2007), the probability for the orientation of a micro-area δA in $d\zeta'_x d\zeta'_y$ is

$$p(\zeta'_x, \zeta'_y) d\zeta'_x d\zeta'_y = \frac{\tau^2}{4\pi\sigma^2} \exp\left(-\frac{\tau^2 \tan^2 \theta_n}{4\sigma^2}\right) \frac{d\Omega_n}{\cos^3 \theta_n} \quad (8)$$

where $d\Omega_n$ is differential solid angle of $\mathbf{n}(\theta_n, \varphi_n)$,

$$d\Omega_n = \sin \theta_n d\theta_n d\varphi_n. \quad (9)$$

Given a micro-area δA (Figure 3), the incident radiance $L_i(\theta_i, \varphi_i)$ and the transmitted radiance $L_o(\theta_o, \varphi_o)$ are related as,

$$\begin{aligned} & L_o(\theta_o, \varphi_o) \cos \beta d\Omega_o \\ &= \bar{F}_i(\alpha, \lambda) L_i(\theta_i, \varphi_i) \delta(\mathbf{n}, \mathbf{e}_i, \mathbf{e}_o) \cos \alpha d\Omega_i \end{aligned} \quad (10)$$

where β is the transmission angle for the incident angle α , $d\Omega_o$ is the solid angle in the transmission

direction, $d\Omega_i$ is the solid angle in the incident direction, and $\bar{F}_i(\alpha, \lambda)$ is the Fresnel coefficient of transmission averaged over polarizations. $\delta(\mathbf{n}, \mathbf{e}_i, \mathbf{e}_o)$ is a Dirac delta function. That is, when \mathbf{n} , \mathbf{e}_i , and \mathbf{e}_o are coplanar and $\sin \alpha = n \sin \beta$ (n is the relative index of refraction), $\delta(\mathbf{n}, \mathbf{e}_i, \mathbf{e}_o) = 1$; otherwise, $\delta(\mathbf{n}, \mathbf{e}_i, \mathbf{e}_o) = 0$. The radiant flux $\delta\Phi(\theta_o, \varphi_o)$ through a micro-area δA is given as

$$\begin{aligned} \delta\Phi(\theta_o, \varphi_o) &= L_o(\theta_o, \varphi_o) \cos \beta \delta A d\Omega_o \\ &= \bar{F}_i(\alpha, \lambda) L_i(\theta_i, \varphi_i) \delta(\mathbf{n}, \mathbf{e}_i, \mathbf{e}_o) \cos \alpha \delta A d\Omega_i \end{aligned} \quad (11)$$

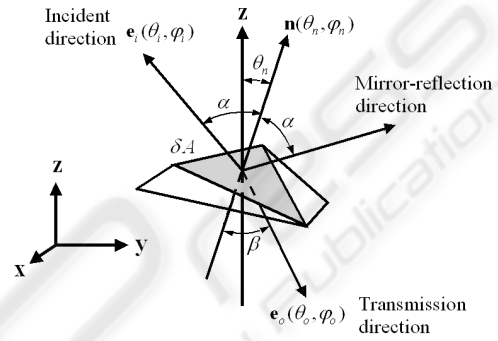


Figure 3: Ray transmission at a micro-area.

Since a local illumination area ΔA over which the BTDF is defined (Figure 1) contains many micro-areas δA , the total radiant flux over ΔA contains contributions from all possible micro-areas,

$$\begin{aligned} \Delta\Phi(\theta_o, \varphi_o) &= \sum_{\delta A} V(\delta A) \delta\Phi(\theta_o, \varphi_o) \\ &= L_i(\theta_i, \varphi_i) \cos \alpha d\Omega_i \sum_{\delta A} V(\delta A) \bar{F}_i(\alpha, \lambda) \delta(\mathbf{n}, \mathbf{e}_i, \mathbf{e}_o) \delta A \end{aligned} \quad (12)$$

where $V(\delta A)$ is a visibility function describing the probability of a micro-area δA that is visible in both directions $\mathbf{e}_i(\theta_i, \varphi_i)$ and $\mathbf{e}_o(\theta_o, \varphi_o)$. The radiance to the transmission direction $\mathbf{e}_o(\theta_o, \varphi_o)$ is given as

$$\begin{aligned} L_o(\theta_o, \varphi_o) &= \frac{\Delta\Phi(\theta_o, \varphi_o)}{\Delta A |\cos \theta_o| d\Omega_o} \\ &= \frac{L_i(\theta_i, \varphi_i) \cos \alpha d\Omega_i \bar{F}_i(\alpha, \lambda)}{|\cos \theta_o| d\Omega_o} \sum_{\delta A} \frac{V(\delta A) \delta(\mathbf{n}, \mathbf{e}_i, \mathbf{e}_o) \delta A}{\Delta A} \end{aligned} \quad (13)$$

Because θ_o is measured from the positive z-axis (see Figure 1) and its value is within $[\pi/2, \pi]$, we take the absolute value of its cosine value in Eq. (13). Substituting Eq. (13) into Eq. (1), we obtain

$$\begin{aligned} \rho_{\text{single}} &= \frac{L_o(\theta_o, \varphi_o)}{L_i(\theta_i, \varphi_i) \cos \theta_i d\Omega_i} \\ &= \frac{\cos \alpha \bar{F}_i(\alpha, \lambda)}{\cos \theta_i |\cos \theta_o| d\Omega_o} \sum_{\text{(over } \zeta)} V(\delta A) \sum_{\text{(fixed } \zeta)} \frac{\delta(\mathbf{n}, \mathbf{e}_i, \mathbf{e}_o) \delta A}{\Delta A} \end{aligned} \quad (14)$$

Here the summation over the local illumination area ΔA has been decomposed into the summation over all micro-areas with fixed height ζ and over

different heights. Since the visibility function $V(\delta A)$ at a fixed height remains the same for given incident and outgoing directions, it has been put outside the inner summation for a fixed height. Considering that the projected area of δA on the $z=0$ plane is

$$(\delta A)^\perp = \delta A \cos \theta_n, \quad (15)$$

where θ_n is the polar angle of the normal $\mathbf{n}(\theta_n, \varphi_n)$ of δA (see Figure 3), the portion of the total projected areas $\sum_{(\text{fixed } \zeta)} (\delta A)^\perp \delta(\mathbf{n}, \mathbf{e}_i, \mathbf{e}_o)$ in ΔA is the probability of a surface point with height in differential interval $[\zeta, \zeta + d\zeta]$ and with orientation in intervals $[\zeta'_x, \zeta'_x + d\zeta'_x]$ and $[\zeta'_y, \zeta'_y + d\zeta'_y]$. Thus,

$$\frac{1}{\Delta A} \sum_{(\text{fixed } \zeta)} (\delta A)^\perp \delta(\mathbf{n}, \mathbf{e}_i, \mathbf{e}_o) = p(\zeta, \zeta'_x, \zeta'_y) d\zeta d\zeta'_x d\zeta'_y \quad (16)$$

From Assumption 5, the combined probability density function can be decomposed as

$$p(\zeta, \zeta'_x, \zeta'_y) = p(\zeta) p(\zeta'_x, \zeta'_y). \quad (17)$$

Applying Eqs. (16,17) into Eq. (14), we obtain

$$\rho_{\text{single}} = \frac{s^2 \cos \alpha \bar{F}_i(\alpha, \lambda) \exp(-s^2 \tan^2 \theta_n / 4)}{4\pi \cos \theta_i |\cos \theta_o| \cos^4 \theta_n} \cdot \frac{d\Omega_n}{d\Omega_o} \int d\zeta p(\zeta) V(\zeta, \mathbf{e}_i, \mathbf{e}_o) \quad (18)$$

This equation may be further expressed as

$$\rho_{\text{single}} = \frac{s^2 \cos \alpha \bar{F}_i(\alpha, \lambda) \exp(-s^2 \tan^2 \theta_n / 4)}{4\pi \cos \theta_i |\cos \theta_o| \cos^4 \theta_n} \cdot \chi(\alpha, \beta) \langle V(\zeta, \mathbf{e}_i, \mathbf{e}_o) \rangle_\zeta \quad (19)$$

where the function $\chi(\alpha, \beta)$ describes $d\Omega_n/d\Omega_o$ (see Appendix), and

$$\langle V(\zeta, \mathbf{e}_i, \mathbf{e}_o) \rangle_\zeta = \int d\zeta p(\zeta) V(\zeta, \mathbf{e}_i, \mathbf{e}_o) \quad (20)$$

is the averaged bistatic visibility function. A bistatic visibility function simultaneously involves the incident direction \mathbf{e}_i and the outgoing direction \mathbf{e}_o . For light transmission, since \mathbf{e}_i points into the original medium and \mathbf{e}_o into the new medium, the correlation between the two directions can be ignored, as stated in Assumption 6. Therefore,

$$V(\zeta, \mathbf{e}_i, \mathbf{e}_o) \approx V(\zeta, \theta_i) V(\zeta, \theta_o), \quad (21)$$

where $V(\zeta, \theta)$ is an individual visibility function that describes the probability of being visible for a ray starting at height ζ and with angle θ (Figure 4), and accordingly,

$$\langle V(\zeta, \mathbf{e}_i, \mathbf{e}_o) \rangle_\zeta \approx \langle V(\zeta, \theta_i) V(\zeta, \theta_o) \rangle_\zeta = \int d\zeta p(\zeta) V(\zeta, \theta_i) V(\zeta, \theta_o) \quad (22)$$

We further approximate Eq. (22) as

$$\langle V(\zeta, \mathbf{e}_i, \mathbf{e}_o) \rangle_\zeta \approx V(0, \theta_i) V(0, \theta_o). \quad (23)$$

where $V(0, \theta_i)$ and $V(0, \theta_o)$ are the individual visibility functions for the incident and outgoing directions when the ray starts from $\zeta = 0$. From the previous study (Sun, 2007),

$$V(0, \theta) \approx \exp\left[-\frac{k_0 \tan \theta}{s} \exp(-s^2 / 4 \tan^2 \theta)\right], \quad (24)$$

where $k_0 = 0.7$. Thus, we finally obtain

$$\rho_{\text{single}} = \frac{s^2 \cos \alpha \bar{F}_i(\alpha, \lambda) \exp(-s^2 \tan^2 \theta_n / 4)}{4\pi \cos \theta_i |\cos \theta_o| \cos^4 \theta_n} \cdot \chi(\alpha, \beta) V(0, \theta_i) V(0, \theta_o) \quad (25)$$

where $\chi(\alpha, \beta)$ is given in the Appendix.

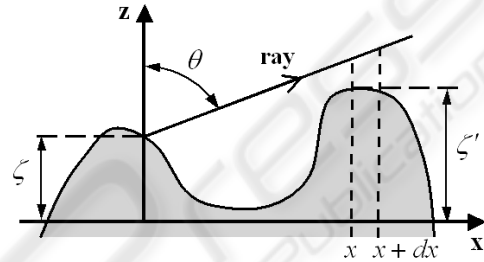


Figure 4: A ray starts at height ζ and with polar angle θ .

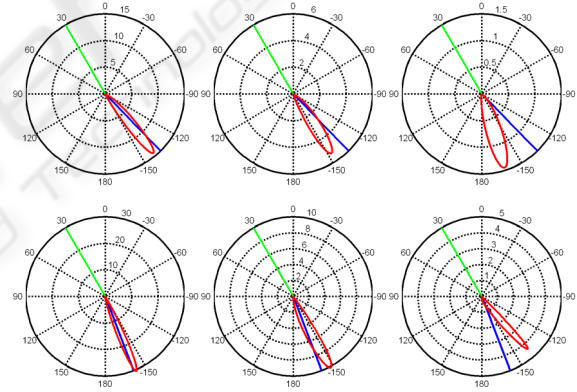


Figure 5: BTDF for different n and s . Parameters are $\theta_i = 30^\circ$, $n = 1/1.4$ for the first row, and $n = 1.4$ for the second row. From the left to right, the values of s are 6, 3, and 1, respectively.

Figure 5 shows ρ_{single} for different values of relative index of refraction (IOR) n and smoothness s . The solid straight lines (in green) in the upper hemisphere indicate the incident direction, and the solid straight lines (in blue) in the lower hemisphere indicate the transmission direction. ρ_{single} has a sharp lobe and shows the off-specular effect. When $n < 1$ (the first row), as the outgoing direction changes from $\theta = -90^\circ$ to $\theta = 180^\circ$, ρ_{single} increases gradually and reaches a maximum, then decreases rapidly.

Also, the direction that ρ_{single} has the maximum shifts toward $\theta=180^\circ$ with the decrease of s . In contrast, for $n>1$ (the second row), when the outgoing direction changes from $\theta=-90^\circ$ to $\theta=180^\circ$, ρ_{single} increases rapidly and reaches the maximum, then decreases gradually. Moreover, the direction for the maximum ρ_{single} shifts toward $\theta=-90^\circ$ with the decrease of s .

The plots in Figure 5 can be explained as below. First, when the surface is smooth, most micro-areas distribute around $\theta_n=0^\circ$ and they contribute to ρ_{single} with $\alpha \rightarrow \theta_i$. Second, Fresnel's transmission coefficient has the maximum for incident angle $\alpha=0^\circ$, and decreases with the increase of α . Therefore, those micro-areas with orientation around the incident direction have large Fresnel's transmission coefficients. These two factors compete with each other. And also, for $n<1$, the refraction angle β is larger than the incident angle α , and vice versa. These result in the plot shapes in Figure 5. With the decrease of s , the maximum distribution of orientations of micro-areas tends to shift from $\theta_n=0^\circ$ toward $\theta_n=90^\circ$, which results in a shift of the direction for the maximum ρ_{single} .

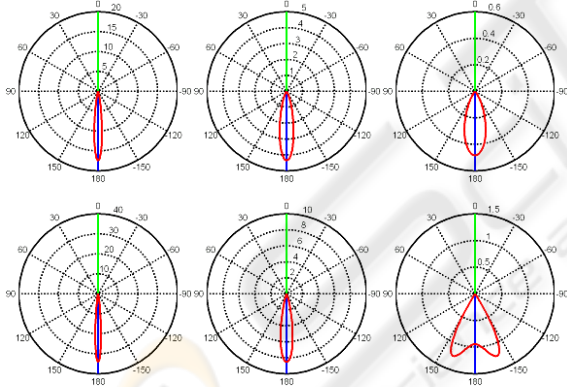


Figure 6: BTDF for different n and s . Here $\theta_i=0^\circ$, and other parameters and notations are the same as Figure 5.

For the normal incidence, ρ_{single} for different values of n and s is shown in Figure 6. For $n<1$, the sharp lobe becomes wider with the decrease of s , as same as Figure 5. However, for the case $n>1$ in both Figures 5 and 6, although the sharp lobes for $s=3$ are all wider than those for $s=6$, the sharp lobes for $s=1$ have different shapes. Consider the rotational geometry, ρ_{single} for $s=1$ in Figure 6 is actually a lobe with an indented peak. We can understand this by the micro-area model. For rough surfaces ($s=1$), most micro-areas distribute with

orientations $\theta_n \square 0^\circ$, and therefore the transmitted light by single scattering tends to travel along the direction with $90^\circ \square \theta_o \square 180^\circ$. This results in the indentation of the lobe in Figure 6. However, the probability of ray blocking is higher for the rays propagating along this direction. This results in the sharper shape for $s=1$ in Figure 5.

4 NUMERICAL SIMULATION

In our Monte Carlo simulation, given a Gaussian rough surface with its mean equal to zero and standard deviation σ , totally N light rays are shot from the incident direction \mathbf{e}_i , each ray carrying a weight W_l ($l=1,2,\dots,N$) that represents its radiance flux intensity. Once a shot ray hits the surface profile, it typically splits into a reflected and a transmitted ray. When the total internal reflection occurs, only a reflected ray is generated.

The surface height at which a shot ray intercepts with the profile is determined by the probability density function of surface height and a generated random number (all the generated random numbers in this paper are uniformly distributed between 0 and 1). The normal direction of this intersection point is obtained by the orientation probability density function with two generated random numbers.

We set the incident flux density to 1. Then the weight of the l th shot ray is given as

$$W_l = V(\zeta_1, \theta_l) \cos \alpha / \cos \theta_n, \quad (26)$$

where ζ_1 is the surface height that the shot ray first intercepts with, α is the incident angle in the local area, and $\cos \theta_n$ is involved because Eq. (16) just describes the probability distribution of δA^\perp at a fixed height.

When a ray with weight W hits the surface profile, it splits into a reflected and transmitted ray, and the weight of the reflected ray is $\bar{F}_r(\alpha, \lambda)W$ and that of the transmitted ray is $\bar{F}_t(\alpha, \lambda)W$. Therefore, after each ray splitting, the generated rays will decrease in intensities. Once the weight of a newly generated ray is lower than the threshold, the tracking process terminates. Otherwise, it will be tracked continuously; whether it is blocked or not depends on its propagation direction, visibility function, and a generated random number.

The radiance to the transmission direction $\mathbf{e}_o(\theta_o, \varphi_o)$ is obtained as

$$L_o = \frac{\sum_{l \in \Delta \Omega_o} W_l}{N \Delta \Omega_o |\cos \theta_o|}, \quad (27)$$

where $\Delta\Omega_o$ is the solid angle along $\mathbf{e}_o(\theta_o, \varphi_o)$, and $\sum_{l \in \Delta\Omega_o} W_l$ calculates the sum of the weights of those rays transmitted into $\Delta\Omega_o$. Consider that the incident irradiance is $\cos\theta_i$ (since incident flux density is set to 1), the BTDF can be calculated by

$$\rho = \frac{\sum_{\Delta\Omega_o} W_l}{N\Delta\Omega_o |\cos\theta_o| |\cos\theta_i|}. \quad (28)$$

In discussion below we may replace ρ with $\rho |\cos\theta_o|$ based on two considerations. First, the previous simulations by Nieto-Vesperinas et al. (1990) calculated the transmitted light intensity, which is proportional to $\rho |\cos\theta_o|$. For convenience of comparing the results, we need to use $\rho |\cos\theta_o|$ instead of ρ . Second, Eq. (28) contains $1/|\cos\theta_o|$ and $\sum_{l \in \Delta\Omega_o} W_l$. When $\theta_o \rightarrow \pi$, $|\cos\theta_o| \rightarrow 0$. However, we cannot take $\Delta\Omega_o \rightarrow 0$ for the calculation of Eq. (28). Therefore, ρ might diverge at $\theta_o \rightarrow 90^\circ$.

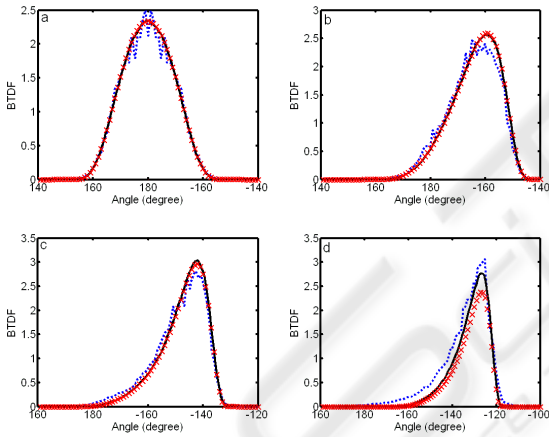


Figure 7: Comparison between our analytical model and simulations. The curves with x marks are from the analytical model, the dot curves from the simulations of Nieto-Vesperinas et al. (1990), and the solid curves from our simulations. Here, $n=1.411$, $s=2.522$, (a) $\theta_i=0^\circ$, (b) $\theta_i=20^\circ$, (c) $\theta_i=40^\circ$, and (d) $\theta_i=60^\circ$.

Figure 7 compares our analytical model and simulations. Nieto-Vesperinas et al. (1990) considered perpendicular and parallel polarizations separately. For comparison, we calculate the average of the two polarizations. In our analytical model and simulation, light intensity can be calculated by $\rho |\cos\theta_o| \Delta A$. Since we do not know the value of ΔA used for the simulation of Nieto-Vesperinas et al., we find it by matching our analytical model with

their results for $\theta_i=0^\circ$. In Figure 7, the comparison shows a very good match.

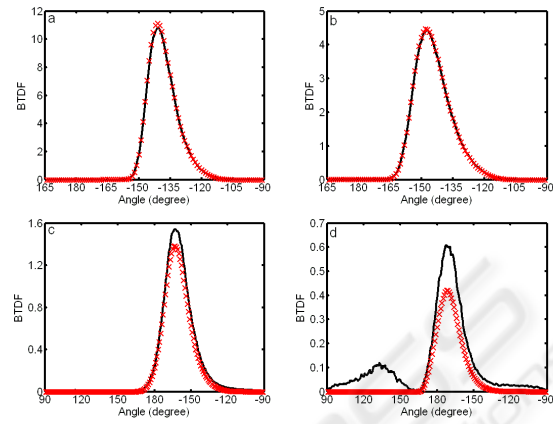


Figure 8: Comparison between simulation and analytical model. The solid curves are from our simulation, and the curves with x marks from analytical model. Here, $\theta_i=30^\circ$, $n=1/1.4$, (a) $s=6$, (b) $s=3$, (c) $s=1$, and (d) $s=0.5$.

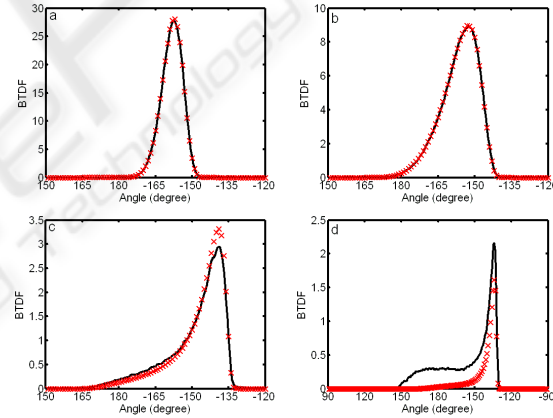


Figure 9: Comparison between simulation and analytical model. The solid curves are from our simulation, and the curves with x marks from analytical model. Here, $\theta_i=30^\circ$, $n=1.4$, (a) $s=6$, (b) $s=3$, (c) $s=1$, and (d) $s=0.5$.

Figures 8 and 9 compare our simulation and the analytical model for different values of n and s . For smooth and moderately smooth surfaces (s is 3 or 6), the analytical model agrees well with the simulation. With small s , the difference between the analytical model and simulation increases. This is because our analytical model only considers single scattering. For smooth surfaces, light transmission is dominated by single scattering. Overall, the model has a good match with the simulation. For rough surfaces (s is small), multiple scattering plays an important role and should be considered.

5 CONCLUSIONS

This paper presents a realistic transmission model of rough surfaces. The model is derived based on the statistical ray method. We have obtained an analytical expression for single scattering. The model has been compared to our Monte Carlo simulations as well as to the simulations by others, and good agreements have been achieved.

In future work, the model can be applied to render realistic transmission effects. The model could be taken into consideration to study object translucency. On simulation to verify the analytical model, we may generate 2D surfaces for given σ and τ , and compute the average of transmission through the surfaces. The current model has not considered multiple scattering, and both the model and simulation have not considered polarization effects. We will consider them in our further work.

REFERENCES

- Ashikhmin, M., Premoze, S., Shirley, P., 2000. A microfacet-based BRDF generator. In *Proc. of ACM SIGGRAPH*, pp. 65-74.
- Beckmann, P., Spizzichino, A., 1963. *The Scattering of Electromagnetic Waves from Rough Surfaces*, Macmillan, New York.
- Blinn, J. F., 1977. Models of light reflection for computer synthesized pictures. In *Proc. Siggraph*, pp. 192-198.
- Cook, R. L., Torrance, K. E., 1982. A reflection model for Computer Graphics. *ACM Transactions on Graphics*, vol. 1, no. 1, pp. 7-24.
- Dorsey, J., Edelman A., Jensen H. W., Legakis J., and Pedersen H. K., 1999. Modeling and rendering of weathered stone. In *Proc. Siggraph '99*, pp. 225-234.
- Fung, A. K., Chen, M. F., 1985. Numerical simulation of scattering from simple and composite random surfaces. *J. Opt. Soc. Am. A*, vol. 2, no. 12, pp. 2274-2284.
- Glassner, A. S., 1995. *Principles of Digital Image Synthesis*, Morgan Kaufmann Publishers, San Francisco, CA.
- Hanrahan, P., and Krueger W., 1993. Reflection from layered surface due to subsurface scattering. In *Proc. Siggraph '93*, pp. 165-174.
- He, X. D., 1993. Physically-based models for the reflection, transmission and subsurface scattering of light by smooth and rough surfaces, with applications to realistic image synthesis. Ph.D thesis, Cornell University, Ithaca, New York.
- He, X. D., Torrance, K. E., Sillion, F. X., Greenberg, D. P., 1991. A comprehensive physical model for light reflection. In *Proc. Siggraph*, pp. 175-186.
- Jensen, H. W., and Christensen P. H., 1998. Efficient Simulation of Light Transport in Scenes with Participating Media Using Photon Maps. *Computer Graphics Proceedings (Proc. SIGGRAPH '98)*, pp. 311-320.
- Jensen H. W., Marschner S. R., Levoy M., and Hanrahan P., 2001. A practical model for subsurface light transport. In *Proc. Siggraph '01*, pp. 511-518.
- Jensen H. W., and Buhler J., 2002. A rapid hierarchical rendering technique for translucent materials. *ACM Trans. Graph.* 21, vol. 3, pp. 576-581.
- Koenderink J., and Doorn A. van., 2001. Shading in the case of translucent objects. In *Proc. SPIE*, vol. 4299, pp. 312-320.
- Kubelka, P., and Munk, F., 1931. Ein Beitrag Zur Optik Der Farbanstriche, *Zeitschrift für Technischen Physik*, p. 593.
- Lafortune, E. P. F., Foo, Sing-Choong, Torrance, K. E., Greenberg, D. P., 1997. Non-linear approximation of reflectance functions. In *Proc. Siggraph*, pp. 117-126.
- Mertens, T., Kautz, J., Bekaert, P., Reeth, F. V., and Seidel, H. -P., 2005. Efficient rendering of local surface scattering. In *Computer Graphics Forum*, vol. 24, pp. 41-49.
- Nieto-Vesperinas, M., Sanchez-Gil, J. A., Sant, A. J., Dainty, J. C., 1990. Light transmission from a randomly rough dielectric diffuser: theoretical and experimental results. *Opt. Lett.*, vol. 18, no. 22, pp. 1261-1263.
- Pharr, M., and Hanrahan, P., 2000. Monte carlo evaluation of non-linear scattering equations for subsurface reflection. In *Proc. Siggraph '00*, pp. 75-84.
- Phong, B., 1975. Illumination for computer generated images. *Comm. of ACM*, vol. 18, no. 6, pp. 311-317.
- Stam, J., 2001. An illumination model for a skin layer bounded by rough surfaces. In *Proceedings the 21th Eurographics Workshop on Rendering Techniques*, pp. 39-52.
- Sun, Y., 2007. Analytical framework for calculating BRDFs of randomly rough surfaces. *J. Opt. Soc. Am. A*, (to appear in March 2007). Currently available online at <http://josaa.osa.org/upcoming.cfm>.
- Torrance, K. Sparrow, E. M., 1967. Theory for off-specular reflection from roughened surfaces. *J. Opt. Soc. Am.*, vol. 57, no. 9, pp. 1105-1114.
- Ward, G. J., 1992. Measuring and modeling anisotropic reflection. In *Proc. SIGGRAPH*, pp. 265-272.
- Wang, R., Tran, J., and Luebke, D., 2005. All-Frequency Interactive Relighting of Translucent Objects with Single and Multiple Scattering, in *ACM Trans. Graphics (Proc. SIGGRAPH '05)*, pp. 1202-1207.

APPENDIX

Here we derive the relationship between the differential solid angles $d\Omega_o$ and $d\Omega_n$. Given an unit sphere (Figure 10), the area $ABCD$ corresponds to $d\Omega_n$ and the area $A'B'C'D'$ to $d\Omega_o$. The points $A, B, A',$ and B' are coplanar, and similarly the points $C, D, C',$ and D' . The planes $ABA'B'$ and $DCD'C'$ intersects at the line POQ , and the angle

between them is $d\gamma$. Therefore, the length of the curve segment AD is

$$|AD| = |AE| \cdot d\gamma = \sin \alpha \cdot d\gamma. \quad (A1)$$

Since $|AB| = d\alpha$, so we obtain

$$d\Omega = |AD| \cdot |AB| = \sin \alpha \cdot d\gamma d\alpha. \quad (A2)$$

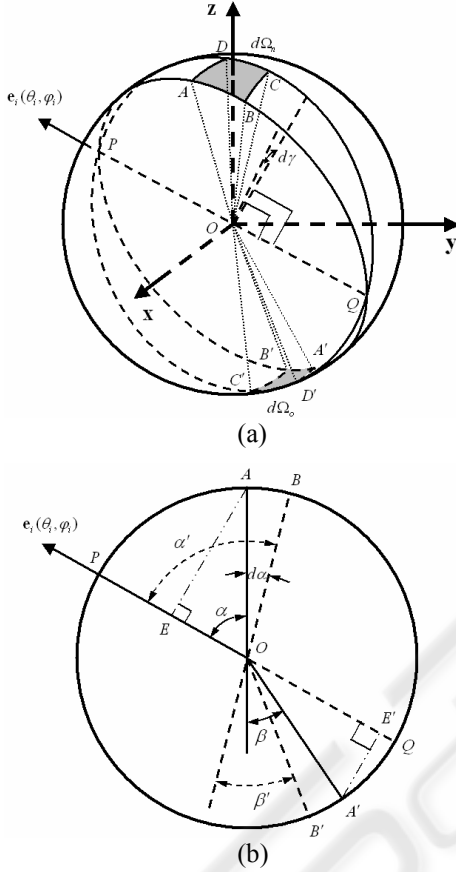


Figure 10: Relationship between $d\Omega_n$ and $d\Omega_o$ ($n > 1$).

The Snell's law gives the following relations:

$$\sin \alpha = n \cdot \sin \beta \quad (A3)$$

and

$$\sin \alpha' = \sin(\alpha + d\alpha) = n \cdot \sin \beta' = n \cdot \sin(\beta + d\beta), \quad (A4)$$

where n is the relative index of refraction ($n > 1$) and $d\beta$ is defined as

$$d\beta = \beta' - \beta. \quad (A5)$$

From Eq. (A4), we can obtain

$$\begin{aligned} & \sin \alpha \cdot \cos(d\alpha) + \cos \alpha \cdot \sin(d\alpha) \\ &= n \cdot [\sin \beta \cdot \cos(d\beta) + \cos \beta \cdot \sin(d\beta)] \end{aligned} \quad (A6)$$

We make the following approximations:

$$\begin{aligned} \cos(d\alpha) &\approx 1, \sin(d\alpha) \approx d\alpha, \\ \cos(d\beta) &\approx 1, \sin(d\beta) \approx d\beta. \end{aligned} \quad (A7)$$

Substituting Eqs. (A3) and (A7) into Eq. (A6), we obtain

$$d\beta = \frac{\cos \alpha}{n \cdot \cos \beta} d\alpha. \quad (A8)$$

From Figure 10(b), we obtain

$$\beta' = \beta - \angle A'OB' + d\alpha. \quad (A9)$$

Therefore, we obtain

$$\angle A'OB' = \left(1 - \frac{\cos \alpha}{n \cdot \cos \beta}\right) d\alpha. \quad (A10)$$

The length of the curve segment $A'B'$ is

$$|A'B'| = \angle A'OB' = \left(1 - \frac{\cos \alpha}{n \cdot \cos \beta}\right) d\alpha. \quad (A11)$$

The length of the curve segment $A'D'$ is

$$\begin{aligned} |A'D'| &= |A'E'| \cdot d\gamma \\ &= \sin(\angle A'OQ) d\gamma = \sin(\alpha - \beta) d\gamma \end{aligned} \quad (A12)$$

Therefore, we obtain

$$\begin{aligned} d\Omega_o &= |A'B'| \cdot |A'D'| \\ &= \left(1 - \frac{\cos \alpha}{n \cos \beta}\right) \sin(\alpha - \beta) d\gamma d\alpha \end{aligned} \quad (A13)$$

Finally, we obtain

$$\chi(\alpha, \beta) \equiv \frac{d\Omega_n}{d\Omega_o} = \frac{\sin \alpha}{\sin(\alpha - \beta)} \left(1 - \frac{\cos \alpha}{n \cdot \cos \beta}\right)^{-1} \quad (A14)$$

Although Eq. (A14) is derived for $n > 1$, it is easy to prove that this expression also holds for $n < 1$.